



CrossMark
click for updates

Cite this: *RSC Adv.*, 2015, 5, 34709

Crystallization and morphology development in polyethylene–octakis(*n*-octadecyldimethylsiloxy)-octasilsesquioxane nanocomposite blends

E. L. Heeley,^{*a} D. J. Hughes,^b P. G. Taylor^a and A. R. Bassindale^a

The dispersion, morphology and crystallization kinetics of low density polyethylene (LDPE)–octakis(*n*-octadecyldimethylsiloxy)octasilsesquioxane (POSS) nanocomposite blends was investigated. Novel octakis(dimethylsiloxy)octasilsesquioxane ($Q_8M_8^H$) molecules were octafunctionalised with octadecyl alkyl-chains (Q_8C_{18}) and blended with 0.25–10 wt% loadings into a commercial LDPE. Time-resolved Small- and Wide-Angle X-ray Scattering (SAXS/WAXS), thermal and microscopy techniques were used to elucidate the POSS dispersal, crystalline morphology and crystallization kinetics of the host polymer. POSS particles dispersed well in the host polymer up to 5% wt loading and acted as nucleating agents without disrupting the crystal lattice of the PE. Above 5% wt loading the POSS aggregated, reduced the bulk crystallinity and hindered the crystallization process. The aggregation of POSS is attributed to increased POSS–POSS interactions whereby the POSS molecules self-assemble in an interdigitated manner. The results were compared with an analogous LDPE– T_8C_{18} POSS cage blend at 10% wt loading. In complete contrast, the T_8 POSS particles disperse well in the host polymer being effective nucleating agents and increased the bulk crystallinity. This may have important implications in the processing of polyolefins where the T_8 system acts to accelerate crystallization whereas the Q_8 system retards it.

Received 21st February 2015
Accepted 7th April 2015

DOI: 10.1039/c5ra03267a

www.rsc.org/advances

Introduction

In the development of nanocomposite functional materials a group of nanosized inorganic–organic hybrid materials known as Polyhedral Oligomeric Silsesquioxanes (POSS)^{1,2} with the general nomenclature $(RSiO_{3/2})_8$, have found widespread use as nanoparticle fillers in polymer materials. There are many studies covering the synthesis and blending of polymer–POSS composites.^{3–10} However, the fundamental issue in developing nanoparticulate composites is the effective dispersal of the nanofiller and hence understanding the effects on the materials properties. These unanswered questions, remain a barrier to the uptake of nanoparticulates in industrial applications.

Cubic POSS molecules denoted as T_8 cages, can be octafunctionalised with pendant R groups attached at the silicon corners of the cage,^{8,11,12} and are the most commonly synthesized and applied systems. However, the analogous Q_8 structures where $Q_8 = R_8(SiO_2)_8$, are now gaining equal attention as potential polymer nanofillers. The Q_8 cages have additional OSiMe₂ spacer groups at each corner of the cage and can be modified by attaching R groups of varying molecular structure to the silicon of the spacer group.^{13–17}

The chemistry of the R groups attached to the POSS cage plays an integral part in the compatibility and hence dispersal of the molecule with the host polymer. For example, non-polar groups such as alkyl and aryl groups can serve as compatible components for polyolefins^{18–22} due to their comparable chemistry, whereas polar groups encourage dispersal in polymers such as polyesters, polyamides, epoxides and polyurethanes.^{23–31} The addition of POSS as nanoparticulate fillers into polymers can bring about changes in the polymer's physical, chemical and mechanical properties, *e.g.* increasing glass transition temperatures, tensile and impact strength, morphology, crystallinity and thermal stability.^{5,7,9,17–30} These changes are usually attributed to the dispersal of the POSS molecules in the amorphous matrix of the host polymer. The dispersal of POSS is dependent on the wt% loading in the host polymer as well as the length and chemistry of the R groups attached to the cage. Dispersed POSS can act as nucleation sites enhancing the polymers crystallization rate under both isothermal and non-isothermal conditions.^{18–22,32} However, increasing the wt% loading of POSS can cause aggregation of the POSS crystals in the polymer matrix, which then retard the crystallization process by hindering the molecular motion of the polymer chains.^{18,21,22}

Many investigations have looked at the influence of varying the length of the alkyl-chain R groups on POSS dispersal, crystallization and physical properties in polyolefins.^{19,33–35} Here, the length of the alkyl-chain played a fundamental role in the POSS dispersion and crystallization kinetics of the host

^aDepartment of Life, Health and Chemical Sciences, Open University, Walton Hall, Milton Keynes, MK7 6AA, UK. E-mail: Ellen.Heeley@open.ac.uk

^bWMG, University of Warwick, Coventry, CV4 7AL, UK



polymer, although the length of the alkyl-chains investigated were relative short (isooctyl being the longest). Recently, we have reported²² on the dispersal, crystallization kinetics and morphology of a series T_8 POSS molecules with long linear alkyl-chain R groups (C_8 , C_{12} and C_{18}) blended at 10% wt fraction into a commercial low density polyethylene (LDPE). The compatibility and dispersal of the POSS molecules increased with increasing alkyl-chain length of the R groups being attributed to improved interaction with the host polymer chains. The POSS molecules acted as nucleating agents increasing the crystallization kinetics and influencing the final polymer morphology.

However, it should be noted that the above cited investigations predominantly report the influence of POSS T_8 cages as nanoparticulate fillers. Fewer reports have detailed the effects of the analogous Q_8 cages in the same manner. The OSiMe₂ spacer groups in Q_8 cage systems, give the R groups greater flexibility in arranging themselves around the POSS core and thus allowing a more efficient packing manner to be achieved, in comparison to the T_8 cage systems. The R groups on one POSS molecule interdigitate to a degree with those on another POSS molecule.^{15,16} Moreover, the degree of interdigitation where the R groups are linear alkyl-chains is seen to increase as the alkyl-chain length increases.¹⁵

Recently, Frone³⁶ and Perrin³⁷ investigated the morphology, thermal and mechanical properties of low density polyethylene (LDPE) blended with a series of Q_8 POSS cages functionalised with linear (up to C_8) and branched alkyl-chain substituents. Interestingly, their studies showed that POSS dispersal increased with increasing alkyl-chain length but, the crystal structure of LDPE was unaltered indicating that the POSS were distributed in the amorphous fraction of the polymer. Generally, they saw a small increase in crystallinity in the composites with linear alkyl-chain groups but the melting and crystallization temperatures of the blends compared with neat LDPE were unchanged, suggesting that the POSS do not act as nucleating agents.

However, to our knowledge, no studies have detailed the crystallization kinetics and morphology development of polyethylene- Q_8 POSS blends where the Q_8 cages have long linear alkyl-chain R groups, that is, beyond C_8 . To address this, we have blended LDPE with novel Q_8 POSS cages octafunctionalised with octadecyl, C_{18} , alkyl-chains, denoted as Q_8C_{18} (octakis(*n*-octadecyldimethylsiloxy)octasilsesquioxane). Previously, the crystal structure and packing morphology of the pure Q_8C_{18} POSS has been fully characterised and compared with the equivalent T_8C_{18} POSS cage system.^{16,38} Both cage systems are crystalline solids but, the molecules self-assemble and pack in a significantly different manner. The long alkyl-chain R groups in both Q_8 and T_8 cage systems align in an axial disposition from the POSS core giving a 'rod-like' self-assembled lamellar packing morphology. However, alkyl chains in the Q_8 cage system can interdigitate and pack efficiently,^{15,16} whereas those in the T_8 system do not. Recently, Hayakawa^{39,40} observed similar self-assembled lamellar type packing morphologies in a series of mono-substituted POSS cages with long aliphatic chains C_6 , C_{12} and C_{18} . In all these cases, the packing length-scales correlate to the overall length-scale of the molecule.

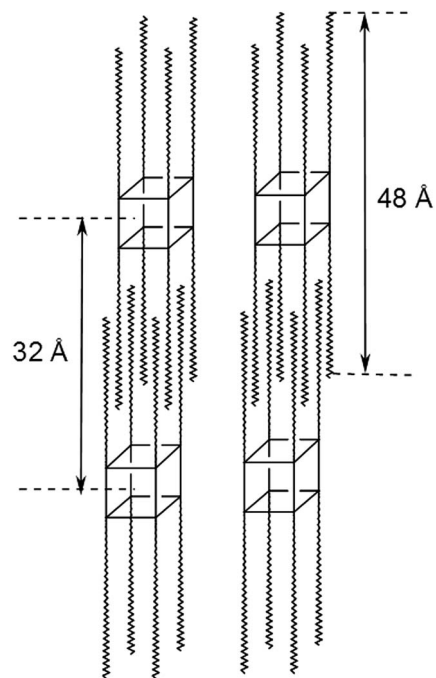


Fig. 1 Packing morphology of the Q_8C_{18} POSS cage system with associated molecular length-scale (48 Å) and repeat interdigitated packing distance (32 Å).¹⁶

Fig. 1 shows the interdigitated packing morphology model for the Q_8C_{18} POSS cage system with associated dimension of the molecule and repeat packing distance.¹⁶

Here, a series of POSS-LDPE blends have been prepared with loadings between 0.25 and 10 wt% of Q_8C_{18} POSS. Using thermal analysis, scanning electron microscopy (SEM) and X-ray diffraction techniques (XRD) we have investigated the dispersion and crystallinity in the blends. Furthermore, isothermal crystallization kinetics, structure development and lamellar morphology of the POSS-LDPE blends were investigated using time-resolved small- and wide-angle X-ray scattering (SAXS/WAXS). We have chosen these techniques for their complimentary nature and power to elucidate the dispersion and the crystallization kinetics of the PE-POSS blends. The scattering techniques are highly sensitive to the dispersal of the POSS in the polymer matrix and reveal the crystalline structure of the blends over a large length-scale; WAXS giving crystal structure of the crystalline lattice and SAXS giving information on the long-range ordering of both the pure PE and POSS and the subsequent blends. These techniques are coupled with SEM and DSC analysis which serve to expand and corroborate the findings from the X-ray analysis.

A comprehensive data set is presented showing how the wt% loading of Q_8C_{18} POSS effects the crystallinity, crystallization kinetics, crystalline morphology and dispersal of the blends compared with the pure LDPE host polymer. The results are then briefly compared and contrasted with the analogous LDPE- T_8C_{18} POSS cage blend at one composition (10% wt loading).²² This has allowed us to ascertain how the packing and



structure differences between the two POSS systems influences the final crystallization and morphology of the host polymer. Hence, indicating which POSS system has the best compatibility and effective nucleating capability for use as potential nanoparticles in polyolefin polymers.

Experimental

Materials

The general synthesis of octakis(*n*-octadecyldimethylsiloxy) octasilsesquioxane, Q₈C₁₈, was achieved by the hydrosilylation of octakis(dimethylsiloxy)octasilsesquioxane with 1-octadecene using Karstedt's catalyst, as detailed in Fig. 2. The full synthetic route, conditions and characterisation of Q₈C₁₈ has been reported in detail elsewhere.¹⁶

The Q₈C₁₈ POSS system was blended with a well characterised commercial low density polyethylene, Lupolen 1840H (GPC $M_w = 250\,000\text{ g mol}^{-1}$, $M_w/M_n = 13.5$, T_m (DSC) $\approx 109\text{ }^\circ\text{C}$), provided by BASF, having both short-chain (30 CH₃/1000 C) and long-chain branching.^{41–43} LDPE–Q₈C₁₈ POSS composites were prepared using a solution compounding method as described previously.^{22,44} The POSS and LDPE were dissolved in CHCl₃ and *para*-xylene solvents respectively, at 95 °C. The two solutions were combined and the resulting mixture stirred at 95 °C for 2 h. The blends produced were then vacuum dried at 130 °C for 10 h. Six blends were prepared with 0.25, 0.5, 1, 2, 5, and 10% wt fraction of Q₈C₁₈ POSS and are identified according to the % wt fraction they contained: PE–Q₈0.25, PE–Q₈0.5, PE–Q₈1, PE–Q₈2, PE–Q₈5, and PE–Q₈10.

Thermal analysis

Differential Scanning Calorimetry (DSC) was performed on each blend using a Mettler Toledo DSC822 instrument under argon gas (flow rate of 80 mL min⁻¹), calibrated with indium metal. Samples (5–20 mg) were loaded into standard 40 μL aluminium pans and heat-cool cycles were run from 25 to 130 °C at a rate of 10 °C min⁻¹. All thermograms and data analysis presented was obtained from the second heat-cool cycle. From the heating cycle the degree of crystallinity X_c , of each blend was determined from the relationship:

$$X_c = \frac{\Delta H_f}{\Delta H_f^0(1 - \phi)} \quad (1)$$

where ΔH_f is the enthalpy of fusion, ΔH_f^0 is the enthalpy of 100% crystalline LDPE⁴⁵ material having a value of 298 J g⁻¹, and ϕ is the wt fraction of Q₈C₁₈ POSS in the blend.

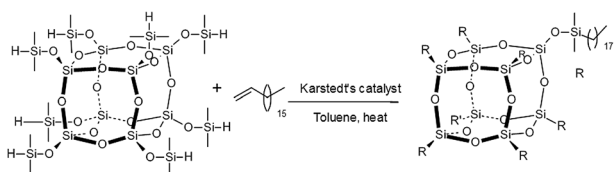


Fig. 2 General synthetic route for the Q₈C₁₈ POSS cage system.¹⁶

Scanning electron microscopy (SEM)

A Zeiss Supra 55VP FEGSEM fitted with an Oxford Instruments Aztec Energy Dispersive Spectroscopy (EDS) system was used to obtain information on the dispersion of POSS, surface texture and elemental composition in the blends at 20 °C. The SEM operating voltage was 10 keV. Samples were sputter coated with gold prior to SEM analysis.

X-ray scattering measurements and data analysis

Static X-ray diffraction (XRD) patterns at 25 °C, were collected on a PANalytical Empyrean diffractometer using Co K_α radiation ($\lambda = 1.79\text{ \AA}$) operating at 40 kV and 40 mA. Samples mounted in flat, circular holders were rotated during the measurement (0.5 s⁻¹). Data were collected on a 1D PIXcel detector system in continuous scanning mode over a scattering angle of $2\theta = 5\text{--}40^\circ$.

Time-resolved Small- and Wide-Angle X-ray Scattering (SAXS/WAXS) measurements were performed at the I22 beamline (Diamond Light Source, Didcot, UK),⁴⁶ with an X-ray energy of 12.4 keV. SAXS data were recorded with a 2D gas-filled multiwire detector⁴⁷ located at a distance of 3.5 m from the sample position and calibrated using an oriented rat-tail collagen specimen. A vacuum chamber was positioned between the sample position and SAXS detector reducing air scattering and absorption. Simultaneous WAXS data were recorded using a 1D detector⁴⁸ situated at the sample position and was calibrated with high density polyethylene.

Isothermal crystallization experiments were performed using a Linkam DSC600 heating stage which was positioned vertically in the incident X-ray beam before the vacuum chamber, as described previously.^{22,49} Samples were sealed in aluminium DSC pans fitted with mica windows (25 μm thickness, 7 mm Ø) and positioned in the heating stage. All samples were heated to 130 °C, held for three minutes and then quenched to the crystallization temperature T_i , at a rate of 50 °C min⁻¹. Simultaneous SAXS/WAXS data collection was started once the crystallization temperature was reached and continued throughout the crystallization process. The data was obtained at a rate of between 8 and 15 s per frame depending on T_i , with a 10 μs wait time.

All SAXS/WAXS data were corrected for sample thickness, transmission, background scattering and any detector spatial distortion. The 2D SAXS data were reduced to 1D intensity plots, $I(q, t)$, by sector averaging symmetrically around the meridian by a fixed angle and radius, q .^{43,50} The peak positions of the 1D SAXS/WAXS data were obtained using a Lorentzian fitting function.

For the isothermal crystallization measurements, the invariant, Q_s , was obtained from the 1D SAXS data where:

$$Q_s(t) = \int_0^\infty q^2 I(q, t) dq \approx \int_{q_1}^{q_2} q^2 I(q, t) dq \quad (2)$$

The data were reduced to integrated intensity I , as a function of scattering vector $q = (4\pi/\lambda) \sin(\theta)$, where 2θ is the scattering angle and λ is the X-ray wavelength. The normalized invariant Q_s , was used to follow the development of the isothermal crystallization process with respect to time at several temperatures.^{22,50}



Avrami plots^{51,52} were obtained for the isothermal crystallization measurements from Q_s , where the Avrami model takes the general form:

$$1 - X_s(t) = e^{-kt^n} \quad (3)$$

Here, $X_s(t) = Q_s(t)/Q_s(\infty)$ is the crystallinity, k is the crystallization rate constant, and n is the Avrami exponent, which can be related to nucleation process and the dimensionality of the growth unit during the isothermal crystallization process. Values of n and k were obtained from Q_s by applying the double logarithmic form of the Avrami equation:

$$\ln(\ln[1 - X_s(t)]) = n \ln t + \ln k \quad (4)$$

where n is the slope of the linear region of the plot and k is the intercept at $t = 1$.

Results and discussion

Thermal analysis

The melting and crystallization behaviour of the PE-POSS blends was investigated using DSC. The heat-cool thermograms of pure PE and PE-POSS blends are shown in Fig. 3. From the thermograms the melting temperatures T_m , crystallization temperatures T_{c1} , and percent crystallinity (determined from the enthalpy of fusion (eqn (1)) that is, ΔH_{c1} at T_{c1}), were obtained and collated in Table 1.

For pure PE the values of T_m and T_c are $\sim 109^\circ\text{C}$ and $\sim 93^\circ\text{C}$ respectively, as indicated by the dashed lines on the thermogram plots in Fig. 3. The PE-POSS blends do not show any significant deviations in the values of T_m and T_c compared with pure PE. Here, it is worth noting that for the pure Q_8C_{18} POSS cage system $T_m = 45.5^\circ\text{C}$ and $T_c = 29.1^\circ\text{C}$ (as previously reported),¹⁶ but there is no evidence of these individual

transitions in any of the PE-POSS thermograms in Fig. 3. Hence, this suggests that the POSS is dispersed in the PE matrix and may not be aggregated into crystals to any large degree.

Similar results have been seen for linear and branched short-chained LDPE- Q_8 blends, where the POSS is assumed to be dispersed in the amorphous phase of the LDPE.^{36,37}

The addition of POSS has a marked effect on the bulk crystallinity of PE, particularly at 10% wt loading. At low wt% POSS (up to 0.5%) the crystallinity increases slightly. However, at 10% wt fraction POSS, there is a significant reduction of the crystallinity compared with pure PE. This indicates that the addition of POSS at very low wt% fraction enhances the crystallization process of PE under non-isothermal conditions. However, as the POSS content is increased the crystallization process is hindered. This postulation is supported by analysis of the crystallization kinetics presented later.

All of the cooling thermograms in Fig. 3, show evidence of a second broad crystallization transition T_{c2} , at $\sim 57^\circ\text{C}$. Table 1 summarises the normalised enthalpy of fusion (that is, ΔH_{c2} at T_{c2}) for this second crystallization transition for pure PE and the blends. The occurrence of the second crystallization transition is commonly seen in LDPEs which have low bulk crystallinity and it is associated with the crystallization of thinner crystal lamellae at lower temperatures whereas the thicker crystal lamellae are formed at higher temperatures.^{36,37,53} Hence, different crystalline fractions are formed as the PE is re-crystallized from the melt. Multiple crystallization transitions are due to the extent of long- and short-chain branching and molecular weight distribution of the PE, both of which are considerable in the LDPE used here.⁴¹⁻⁴³ Here, the enthalpy change associated with the second crystallization transition is greatest for pure PE and reduces with increasing POSS content of the blends. Thus, generally as the wt% fraction of POSS increases the formation of the thinner less well defined crystallites decreases. This is generally mirrored in the reduction of overall bulk crystallinity as the wt% fraction of POSS increases as well; once more highlighting the fact that at higher wt% fractions of POSS, the molecules in the blend may hinder the crystallization of the PE. Again, comparable results have been reported, where a lower proportion of thinner lamellae crystals form in the secondary crystallization process in the PE-POSS blends compared with pure PE.^{36,37}

From the DSC analysis of the PE-POSS blends, an increase in the bulk crystallinity is seen compared to pure PE, at very low wt% fractions of POSS. However, as the POSS content increases the crystallinity is significantly reduced and any secondary crystallization is also reduced. These results initially indicate that POSS dispersed in the PE matrix at low levels, may potentially act as a nucleating agent for the crystallization process whereas, at high levels POSS suppresses crystallization. It is worth noting that this notion is supported by the following X-ray scattering data.

X-ray scattering measurements

Static 1D SAXS and XRD scans of pure PE, pure Q_8C_{18} POSS and PE-POSS blends at 25°C are shown in Fig. 4. At this

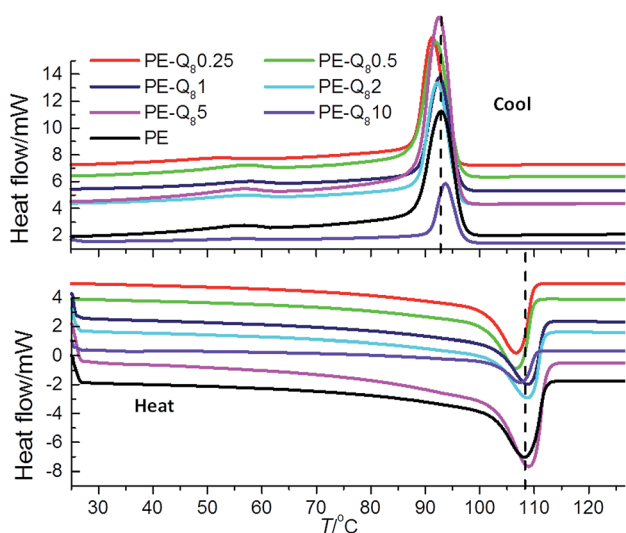


Fig. 3 DSC heat-cool thermograms of pure PE and PE-POSS blends. Data are vertically off-set for clarity. A dashed line on heat-cool thermograms indicates the T_m and T_c of pure PE at 108.7°C and 92.9°C , respectively.



Table 1 DSC melting temperature T_m , crystallization temperature T_c , and % crystallinity of PE and PE–POSS blends

| Sample | T_m /°C | T_{c1} /°C | ΔH_{c1} /J g ⁻¹ at T_{c1} /°C | ΔH_{c2} /J g ⁻¹ at T_{c2} /°C | % crystallinity |
|------------------------|-----------|--------------|--|--|-----------------|
| Pure LDPE | 109 | 93 | 56 | 2.8 | 36.7 |
| PE–Q ₈ 0.25 | 107 | 91 | 52 | 2.6 | 39.0 |
| PE–Q ₈ 0.5 | 107 | 92 | 58 | 2.3 | 38.6 |
| PE–Q ₈ 1 | 109 | 93 | 58 | 1.9 | 35.0 |
| PE–Q ₈ 2 | 109 | 92 | 57 | 1.3 | 34.5 |
| PE–Q ₈ 5 | 109 | 93 | 57 | 1.2 | 36.5 |
| PE–Q ₈ 10 | 108 | 94 | 57 | 0.9 | 31.1 |

temperature all samples (both PE and the Q₈C₁₈ POSS) are well below their melt and crystallization temperatures so are considered crystalline.

Firstly, the SAXS and XRD of the pure Q₈C₁₈ POSS are shown in Fig. 4A and B respectively, where the SAXS data provides detail on the long-range ordering and molecular length-scale of POSS and the XRD about the crystal lattice structure. The SAXS shows a strong 1st order peak at a length-scale of 32 Å and is related to the overall dimension of the packing of the POSS cage when the long alkyl-chain groups are interdigitated (shown schematically in Fig. 1).¹⁶ The XRD for the pure POSS which is a waxy solid at room temperature, with a melt temperature of 45.5 °C, shows a group of prominent peaks (labelled P2–P4) in the 2θ region of 24–27° previously assigned to the distance between the POSS cages and intra and inter chain packing distances.^{8,12,16,54} The peak at ~20° (labelled P1), is attributed to the diagonal dimension of the POSS cube body.^{8,15–17}

Fig. 4C and D show the 1D SAXS and XRD for pure PE and PE–POSS blends respectively. For pure PE the SAXS data shows a broad scattering maximum or long period (L_p) at ~200 Å, which is representative of the average length-scale of crystalline and amorphous layer thicknesses or lamellar repeat distance.^{22,43} The PE–POSS blends also show the scattering maximum at ~200 Å of PE without any shift in d -spacing.

However, a second weak scattering peak is seen in the 5% and 10% PE–POSS blends at 32 Å. This corresponds to the 1st order peak of pure POSS (Fig. 4A) indicating that the pure POSS particles seem to aggregate in the PE matrix in these particular blends showing some self-assembly and long-range ordering.¹⁶ The 1st order peak is not evident in the other blends where the wt% fraction is less than 5%, which suggests that there is improved dispersal of POSS particles in the PE amorphous matrix and any significant aggregation is not observed.

In Fig. 4D, the two main XRD peaks are common in all scans and labelled as (110) and (200) at 2θ values of 25° and 27.5° respectively. These are associated with the orthorhombic structure of polyethylene. These two peaks are in a similar region to the main group of peaks in the pure POSS in Fig. 4B (24–27°). The (110) and (200) peaks do not shift in the XRD scans of the PE–POSS blends compared with the pure PE, so we assume that the PE crystal lattice is not distorted by the addition of the POSS particles at any of the wt% fractions investigated. Similar results are seen for shorter linear and branched chained LDPE–Q₈ blends.^{36,37} Also, no other POSS crystal peaks (from Fig. 4B) are evident in the PE–POSS blend XRD scans. This suggests that the POSS is dispersed in the amorphous regions of the PE in the blends when in its crystalline form, and even at a loading of 10%, no large regular crystalline aggregates of POSS molecules in the blend is observed.

Time-resolved SAXS/WAXS measurements

The pure PE and blends were isothermally crystallized at several temperatures from 95 °C to 100 °C which is just below T_m for PE = 109 °C, however these temperatures were well above the Q₈C₁₈ POSS melt temperature. Hence, at these temperatures the crystalline structure development of just the PE was followed with simultaneous SAXS/WAXS as the POSS component will not crystallize at such high temperatures, so are considered as being in the melt form.

To show the difference in the development of the long-range order and crystalline structure the last SAXS/WAXS data frames for pure PE and the blends from the isothermal crystallizations at 95 °C and 100 °C are given in Fig. 5.

In Fig. 5A, a broad SAXS peak is seen for PE and all the blends at 95 °C, but the final d -spacing or long period, L_p (PE being ~350 Å indicated by dashed line in figure) is seen to shift slightly in the blends. A reduction in the L_p of the blends is seen between wt% loadings of 0.5 and 2%, indicating an insertion of narrow lamellae.^{22,43} Blends of 5% and 10%, show an increase in

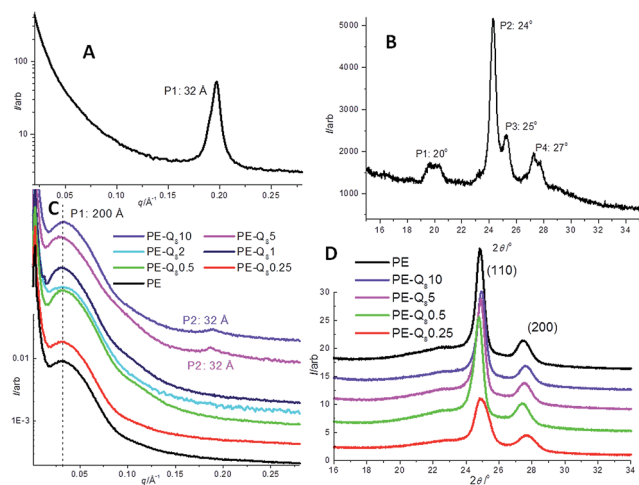


Fig. 4 Static SAXS and XRD scans for pure PE and PE–POSS blends at 25 °C. (A) SAXS of pure Q₈C₁₈ POSS; (B) XRD of pure Q₈C₁₈ POSS; (C) SAXS of pure PE and PE–POSS blends; (D) XRD of pure PE and selected PE–POSS blends. Data in all plots are vertically off-set for clarity.



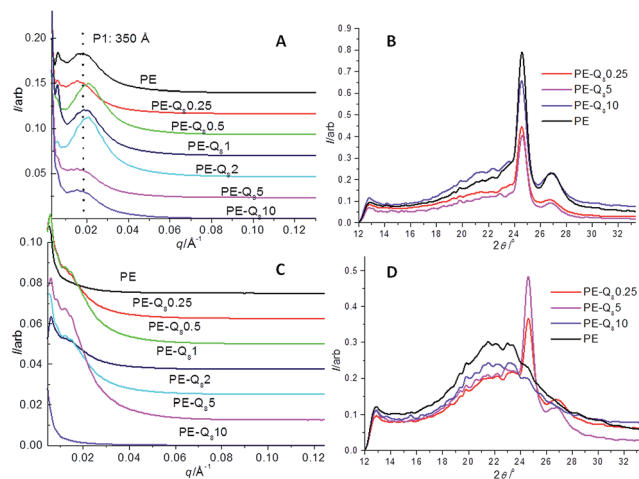


Fig. 5 Final 1D SAXS/WAXS frames for pure PE and selected blends. (A) and (B) SAXS/WAXS for PE and blends at 95 °C, respectively; (C) and (D) SAXS/WAXS for PE and blends at 100 °C, respectively. Data are off-set for clarity on the vertical axis.

L_p compared with the pure PE, indicating larger amorphous regions and imperfect crystal lamellae regions. Hence, low wt% loading of the POSS in the PE amorphous regions, nucleates smaller lamellae to grow and increases crystallinity (supporting the DSC analysis of % bulk crystallinity, Table 1). At higher wt% loading, a less well developed crystalline lamellae structure prevails, where the POSS molecules in the PE amorphous matrix hinder the crystallization of the PE molecules. Again DSC data indicates lower % bulk crystallinity in these blends.

Corresponding WAXS data for PE at 95 °C and selected blends is given in Fig. 5B. Here, the (110) and (200) peaks are clearly well developed signifying the crystalline structure of PE. In contrast, Fig. 5C and D show the final SAXS/WAXS data respectively, for PE and the blends once isothermally crystallized at 100 °C. The SAXS peaks, if evident at this temperature, tend to manifest as a shoulder of intensity towards the back-stop, having shifted to low q (very large d -spacings) suggesting the lamellar morphology is poorly developed, with large amorphous regions and imperfect lamellae crystals.⁴³ In fact, no real discernible peak is seen for PE and the PE-Q₈10 blend. This is also mirrored in the WAXS, where the (110) and (200) peaks are not observed on the amorphous background, indicating no real crystalline structure has developed in the PE. Again at these temperatures the POSS molecules reside in melt form in the amorphous PE matrix and hinder the PE crystals to form.

Crystallization kinetics and Avrami analysis of time-resolved SAXS data

Fig. 6 shows the normalized isothermal crystallization curves obtained from the invariant SAXS data (eqn (2)), for pure PE selected blends. The crystallization process is slower as the isothermal temperature increases.

These plots are used to obtain the crystallization half-time $t_{1/2}$, which represents the time taken to reach 50% conversion

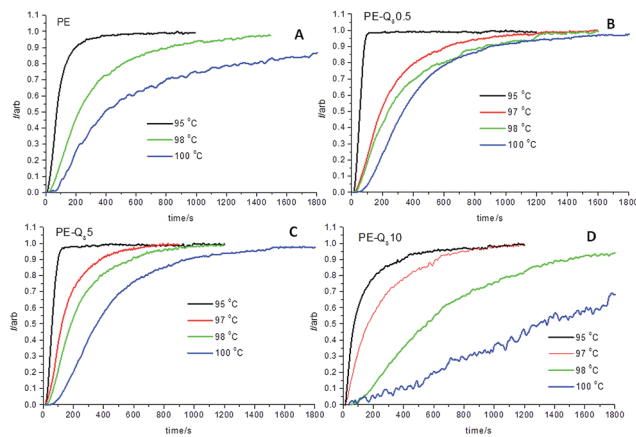


Fig. 6 Isothermal crystallization curves at several temperatures for pure PE and selected blends from the time-resolved SAXS invariant data. (A) Pure PE; (B) PE-Q₈0.5 blend; (C) PE-Q₈5 blend; (D) PE-Q₈10 blend.

to full crystallinity at a specific temperature.^{22,50} In Fig. 6, the PE-Q₈10 blend shows significantly slower crystallization kinetics than the pure PE and other blends at low under-coolings. Comparing the crystallization half-times $t_{1/2}$, in Fig. 7, for PE and the blends shows the variation in the crystallization rates more clearly.

The variation in $t_{1/2}$ in Fig. 7, shows that pure PE has slower crystallization kinetics compared with most of the blends. Thus, it is reasonable to assume that the POSS particles in the blends act as nucleating agents. However, the PE-Q₈10 blend shows that at this level of wt% loading the POSS particles are hindering the crystallization process at higher temperatures. This fits with the lack of crystalline structure development in this blend at 100 °C, indicated by SAXS/WAXS data (Fig. 5) and low overall bulk crystallinity from DSC analysis.

Avrami plots from the double logarithmic form of the Avrami equation (eqn (4)) were obtained from the isothermal crystallization curves for all samples at each isothermal crystallization temperature. Fig. 8, shows the Avrami plots with fits to the linear regions at 95 °C.

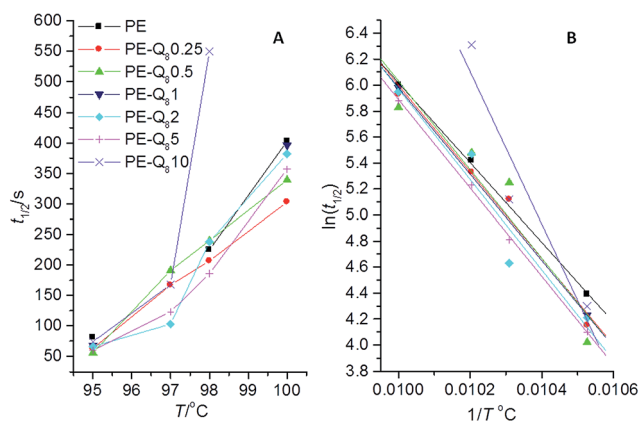


Fig. 7 (A) Crystallization half-times ($t_{1/2}$) versus temperature for pure PE and blends; (B) corresponding plots of $\ln(t_{1/2})$ versus $1/T$.



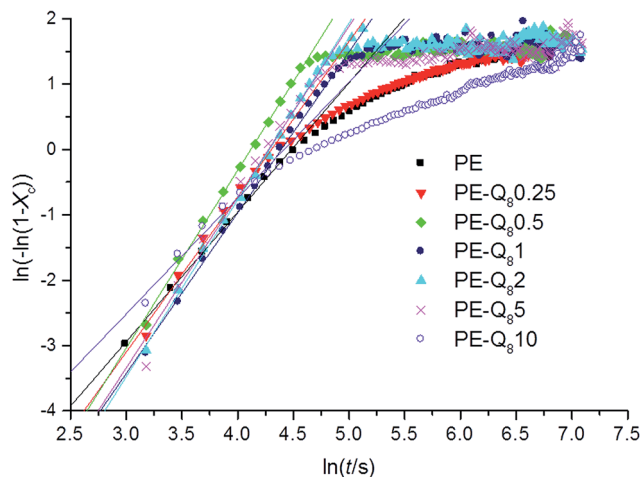


Fig. 8 Avrami plots and fits to the linear regions for pure PE and blends during isothermal crystallization at 95 °C.

In pure PE, the fitted linear region of the Avrami plot correlates to the primary crystallization process. This is followed by the slower secondary crystallization process.^{51,52} On addition of small wt% of POSS, the primary process dominates and the overall crystallization time is reduced. However, for 10% wt POSS loading, the secondary crystallization process is similar to pure PE but proceeds at a slower rate. This supports the earlier argument, where lower wt% of POSS acts as a nucleating agent whereas, higher wt% POSS retards crystallization and reduces the overall crystallinity.

The Avrami exponent n is obtained from the linear fit region and the rate constant, $\ln k$, from the intercept. Table 2, collates all the Avrami parameters obtained from the Avrami plot fits as well as $t_{1/2}$ values, for pure PE and the blends during isothermal crystallization at several temperatures.

The Avrami exponent n , provides information about the nucleation and dimensionality of the crystal growth unit of the material during the isothermal crystallization process. For pure PE n is in the range of 1.4 to 2 with decreasing isothermal crystallization temperature. Values of n in the region of 2–4 have previously been reported for HDPE–POSS blends during isothermal and non-isothermal crystallization.^{21,55,56} Values of $n \leq 2$ implies a low dimensionality growth unit; homogeneous or heterogeneous nucleation of fibril or disc like structures.^{57–59} The Avrami exponents for the blends are still relatively low in, the region of 2–4, but on average a slight increase compared to the pure PE is seen in the values. This indicates that the POSS particles in the blends do seem to increase the dimensionality of the growth unit and are therefore likely to act as heterogeneous nucleation sites. In all cases the rate constant k , decreases with increasing isothermal crystallization temperature.

SEM of PE–POSS blends

To investigate the dispersal of the POSS in the PE matrix, SEM and elemental analysis on the PE–Q₈10 and PE–Q₈1 blends was performed at 20 °C. This is comparable to the static SAXS and

Table 2 Crystallization half-times ($t_{1/2}$) and Avrami parameters for pure PE and the blends at several isothermal crystallization temperatures

| Sample | $T_i/^\circ\text{C}$ | $t_{1/2}/\text{s}$ | Avrami exponent, n | $\ln(k/\text{s}^{-1})$ | |
|------------------------|----------------------|--------------------|----------------------|------------------------|-------|
| PE | 95 | 81 | 2.0 | −8.9 | |
| | 98 | 225 | 1.6 | −9.1 | |
| | 100 | 403 | 1.4 | −9.6 | |
| PE–Q ₈ 0.25 | 95 | 63 | 2.4 | −10.2 | |
| | 97 | 167 | 2.3 | −11.3 | |
| | 98 | 207 | 2.2 | −11.4 | |
| | 100 | 378 | 2.8 | −16.4 | |
| PE–Q ₈ 0.5 | 95 | 56 | 2.7 | −11.2 | |
| | 97 | 191 | 2.1 | −11.3 | |
| | 98 | 240 | 2.0 | −11.1 | |
| | 100 | 339 | 3.3 | −18.9 | |
| PE–Q ₈ 1 | 95 | 68 | 2.5 | −10.8 | |
| | 100 | 396 | 2.3 | −14.3 | |
| | PE–Q ₈ 2 | 95 | 68 | 2.7 | −11.6 |
| | | 97 | 103 | 2.4 | −11.6 |
| 98 | | 238 | 2.4 | −12.6 | |
| 100 | | 382 | 2.8 | −15.8 | |
| PE–Q ₈ 5 | 95 | 60 | 2.6 | −10.4 | |
| | 97 | 123 | 2.1 | −11.1 | |
| | 98 | 186 | 2.7 | −13.6 | |
| | 100 | 357 | 3.7 | −20.4 | |
| PE–Q ₈ 10 | 95 | 74 | 1.8 | −7.8 | |
| | 97 | 168 | 1.4 | −7.2 | |
| | 98 | 550 | 2.4 | −14.8 | |

XRD data shown in Fig. 4 where the POSS and PE is fully crystallised at room temperature.

From the static SAXS data (Fig. 4C) the PE–Q₈10 blend showed the 1st order scattering peak of the POSS indicating aggregation of the POSS particles, whereas this peak was not evident in low wt% loadings of POSS in the PE matrix. This is confirmed in the SEM in Fig. 9.

The SEM image for the PE–Q₈10 blend shows a spherical feature which is an aggregation of POSS particles in the PE matrix. The locations of the X-ray elemental analysis are labelled in the SEM image and the spectral data of the elemental analysis are given in Table 3.

The elemental analysis of spectrum 3 (an area of the PE matrix) indicates mostly carbon as expected from the pure PE, as well as significant amounts of silicon and oxygen from the

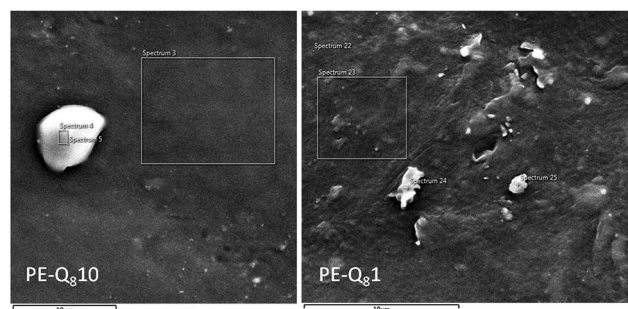


Fig. 9 SEM images of PE–Q₈10 and PE–Q₈1 blends at 20 °C. X-Ray EDS spectrum location points and areas are indicated.



Table 3 X-ray elemental analysis of SEM images for PE-Q₈1 and PE-Q₈10 blends

| Spectrum | Element | wt% |
|----------------------------------|---------|------|
| PE-Q ₈ 10: spectrum 3 | C | 84.9 |
| | O | 9.8 |
| | Si | 5.3 |
| PE-Q ₈ 10: spectrum 4 | C | 47.5 |
| | O | 21.7 |
| | Si | 30.9 |
| PE-Q ₈ 10: spectrum 5 | C | 41.2 |
| | O | 15.3 |
| | Si | 43.5 |
| PE-Q ₈ 1: spectrum 23 | C | 99.1 |
| | O | 0.9 |
| PE-Q ₈ 1: spectrum 24 | C | 97.8 |
| | O | 2.0 |
| | Si | 0.2 |
| PE-Q ₈ 1: spectrum 25 | C | 98.7 |
| | O | 1.2 |
| | Si | 0.1 |

POSS distributed in the matrix. Elemental analysis of the particle feature (spectra 4 and 5) shows high levels of silicon and oxygen which confirms that this is an aggregation of POSS particles; as expected from the SAXS data.

In contrast the SEM image for the PE-Q₈1 blend shows some particulate features in the matrix. However, elemental analysis of the matrix and particles shows mainly carbon with a little silicon and oxygen. Thus, POSS is not sufficiently aggregated at such low wt% loadings in this blend, but is most likely dispersed in the PE amorphous matrix. Again from the SAXS data, this is expected as low wt% loadings of POSS are well dispersed in the PE matrix.

General discussion and comparison of PE-Q₈C₁₈ and PE-T₈C₁₈ blends

The data presented here has shown that blending Q₈C₁₈ POSS in PE clearly influences the crystalline lamellar morphology and crystallization kinetics of the polymer. As the wt% loading of POSS is increased it is apparent that the POSS begins to aggregate and hinders the crystallization of the PE, especially at the highest wt% loading of 10%. This was shown by the reduction of the bulk crystallinity from DSC, lack of crystalline morphology from SAXS/WAXS data and elemental analysis from SEM. Thus, the POSS-POSS interactions increase as the wt% loading increases, and poor dispersal is observed in the polymer matrix leading to POSS aggregation. Again, this is supported by the emergence of the 1st order SAXS peaks for the self-assembled pure POSS at 32 Å, in the blends at 5 and 10 wt%. This also fits with the proposed packing model (Fig. 1), which has been observed for pure Q₈C₁₈ POSS,¹⁶ as depicted in Fig. 4A, where the crystalline POSS molecules are interdigitated.

The observed effects of POSS either nucleating or hindering the crystallization kinetics of the PE can be interpreted on a molecular level. Here, from the SAXS and SEM data at 25 °C, aggregation and phase-separation has been observed with increasing wt% POSS blended in the PE. This is attributed to

POSS aggregations that disrupt the PE crystallization kinetics and perfection of the crystallites, but do not distort the PE crystal lattice being contained within the amorphous matrix.

The POSS molecules at high wt% loadings aggregate and reside in the amorphous polymer matrix and at the isothermal crystallization temperatures investigated, the POSS are in the melt form. The POSS disrupt the molecular motion of the polymer chains, hence retarding crystallization kinetics (as shown with the isothermal crystallization SAXS/WAXS data) and reduces the growth of the crystallites. Once the blend is cooled the POSS molecules crystallise and phase-separate out.

Conversely, at lower wt% loadings the POSS molecules are again distributed in the amorphous matrix, but are not concentrated enough to aggregate effectively and do not phase-separate out once fully cooled to room temperature. From the time-resolved SAXS/WAXS data, at low wt% POSS can act as nucleation points giving increased crystallization kinetics of the polymer during crystallization at high temperatures and serve as sites where new lamellae can begin to grow.

This crystallization behaviour has also been seen in other POSS-polyolefin (PE and iPP)-POSS blends; albeit with different types of POSS than those studied here (T₈ rather than Q₈). Waddon^{20,60} reported similar types of behaviour for PE copolymer-POSS blends where aggregates of both PE and POSS were observed when crystallized from the melt and POSS disrupted the crystallization process. X-ray scattering studies confirmed the presence of POSS and PE crystal structures but the PE lattice was not distorted by POSS, implying that the POSS and PE form a two-phase crystalline structure. Fu¹⁸ and Joshi^{21,55} also studied the isothermal crystallization kinetics in PP-octamethyl and HDPE-octamethyl POSS blends respectively. Here again they observed that higher POSS fractions in the blend reduced the crystallization kinetics due to the dispersal of POSS molecules in the polymer matrix retarding the molecular motion of the chains and hence, decreases crystal growth. Recently, Huang^{61,62} studied the crystallization kinetics of POSS-polydimethylsiloxane rubber (PDMS) nanocomposite blends. Once again they reported that at low loadings POSS was uniformly dispersed in the polymer matrix and acted as nucleation agents, but as the POSS aggregate at higher loadings they crystallize in regions restricting the PDMS chain segments from forming ordered structures.

All of these comparative studies indicate that at high levels of POSS loadings, POSS aggregate as the POSS-POSS interactions are greater than POSS-polymer interactions at a molecular level. The POSS molecules phase-separate out of the polymer matrix, this in effect, hinders the crystallization kinetics of the host polymer. However, at low loadings of POSS, the POSS-polymer interactions are greater and hence the POSS are preferentially dispersed in the polymer matrix. Thus, the POSS molecules do not aggregate or phase-separate out but act as nucleating agents for the host polymer during crystallization. These observations are corroborated by our findings here with the Q₈C₁₈ PE-POSS blends.

At this point it is interesting to compare these results briefly with those of the analogous T₈C₁₈ POSS-PE blends,²² where the POSS molecules do not have the OSiMe₂ spacer groups and so the C₁₈ alkyl chains are directly attached to the corners of the



cage. The T_8C_{18} cages do not interdigitate (in contrast to the Q_8C_{18} molecules, Fig. 1), but form rod-like bundles which stack in a regular bilayer structure, with a packing distance of 52 Å (ref. 16, 38 and 54) assigned to the molecular length-scale of the POSS molecule. The different packing scenarios are attributed to the added flexibility of the alkyl-chains in the Q_8 cages, due to the OSiMe₂ spacer groups.

Similarly, we have reported on the morphology and crystallization kinetics of PE where T_8C_{18} POSS particles have been blended into PE at a 10% loading²² (PE- T_8 10). Interestingly, we now observe contrasting results with respect to the two POSS blend systems. The POSS in the PE- T_8 10 POSS blend showed good dispersal in the matrix from both DSC and X-ray analysis. The PE- T_8 10 POSS blend showed a significant increase in crystallinity at ~42% (where pure PE is ~37%), compared with the reduction seen here with the PE- Q_8 10 blend at ~31%. The increased dispersal and crystallinity in the PE- T_8 10 POSS blend is also highlighted in Fig. 10.

This shows the static SAXS at 25 °C, where the PE- Q_8 10 blend shows the separate 1st order peak of pure Q_8C_{18} POSS, in contrast no similar 1st order peak at ~52 Å ($q = 0.121 \text{ \AA}^{-1}$) for T_8C_{18} is observed in the PE- T_8 10 blend.³⁸ This again confirms that the T_8C_{18} POSS is well dispersed in the blend at 10% loading, whereas the Q_8C_{18} is aggregated at this loading. The lamellar morphology is also significantly altered; pure PE and PE- Q_8 10 blend have a final $L_p = 200 \text{ \AA}$ but this is significantly reduced in the PE- T_8 10 blend where the final $L_p = 155 \text{ \AA}$.²² The reduction in L_p and increased bulk crystallinity in the PE- T_8 10 blend indicates shorter average amorphous and lamellar crystal repeat distances, from insertion and subsequent growth of lamellae into the amorphous regions. This is in contrast for the PE- Q_8 10 blend where the existence of a second crystalline transition T_{c2} (Fig. 3 and Table 1) highlighted by the insertion of thinner lamellae into the amorphous polymer, is significantly reduced for this blend.

Finally, a comparison of isothermal crystallization kinetics also emphasizes the difference in the Q_8 and T_8 blends. Fig. 11,

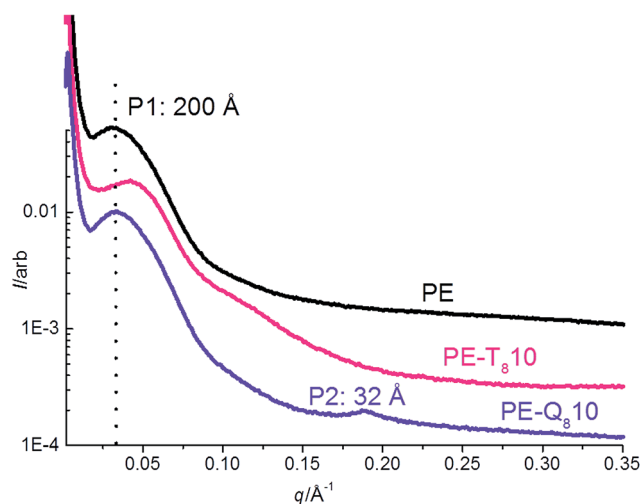


Fig. 10 Comparison of static SAXS data at 25 °C of pure PE and 10% blends of PE- T_8C_{18} and PE- Q_8C_{18} .

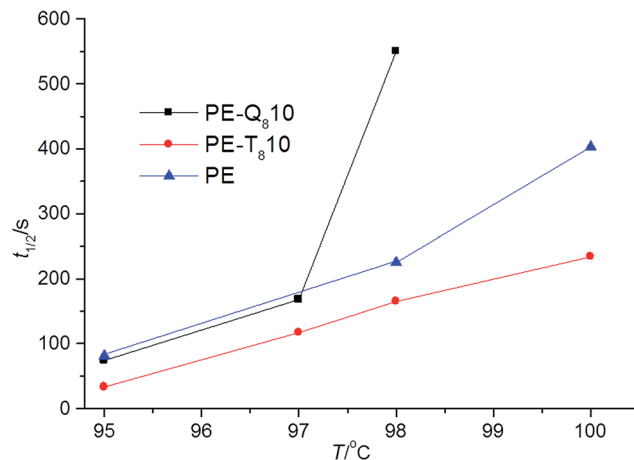


Fig. 11 Comparison of $t_{1/2}$ pure PE and 10% blends of PE- T_8C_{18} and PE- Q_8C_{18} at several isothermal crystallization temperatures.

presents the crystallization half-times $t_{1/2}$, for pure PE and 10% blends of PE- T_8C_{18} and PE- Q_8C_{18} at several isothermal crystallization temperatures.

Clearly, pure PE and PE- Q_8C_{18} blend have similar values of $t_{1/2}$ up to undercoolings of ~97 °C but, at undercoolings above ~97 °C the kinetics are slowed significantly, compared with pure PE for this blend. However, at all undercoolings, the PE- T_8C_{18} blend shows increased crystallization kinetics, more so for both the pure PE and the PE- Q_8C_{18} blend.

The comparison of the PE- T_8C_{18} and PE- Q_8C_{18} blends with respect to each other and pure PE gives rise to some noteworthy points. The dispersal, crystallinity and crystallization kinetics are all increased in the T_8 POSS cage blends compared with both pure PE and comparable Q_8 POSS blends. Evidently, this difference is due to the different structural chemistry of the Q_8 POSS cages, that is, the additional OSiMe₂ spacer groups, as in both cases the C_{18} alkyl-chain group is the same. The added flexibility of the OSiMe₂ spacer groups allows the interdigitation of the alkyl-chains attached to the POSS molecules, which in turn promotes preferred POSS-POSS interaction and aggregation as the wt% loading increases in the blend.

This aggregation appears to then hinder the crystallization process in the host polymer, PE. A distinctly different situation is seen with the T_8C_{18} POSS system. This has good dispersal and increases the crystallization kinetics and crystallinity in PE, where the POSS act as nucleating agents.²² Indeed, T_8C_{18} POSS cages do not interdigitate so the POSS-POSS interaction at higher wt% loadings is not significant enough to cause aggregation (at least at loadings of 10% as studied here).

Conclusions

We have investigated the dispersal, morphology and crystallization kinetics of a series of novel PE- Q_8C_{18} POSS blends with increasing wt% loadings. From the X-ray and DSC results, as the wt% loading of POSS in the PE matrix is increased the dispersal of the POSS is reduced and hinders the crystallization kinetics and hence lowers the bulk crystallinity of the PE. Aggregation of



POSS is observed from 5% loading, where POSS–POSS interactions are favoured and the molecules self-assemble in an interdigitated manner and phase-separate out of the host polymer matrix. At low loadings, the POSS is well dispersed and an increase in both the bulk crystallinity and crystallization kinetics are observed, where the POSS acts as a nucleating agent. The POSS do not aggregate or phase-separate out of the host polymer matrix.

A comparison is also made with the analogous T_8C_{18} POSS cage system when blended in the same PE at 10% loading. Interestingly, the Q_8 and T_8 systems give contrasting results, which are attributed to their different structural chemistry; that is, from the added flexibility of the alkyl-chain groups attached to the Q_8 POSS cages owing to the $OSiMe_2$ spacer groups, which are absent in the T_8 cage systems. Both the T_8 and Q_8 POSS particles do not significantly alter the melting and crystallization temperatures of the host polymer, but T_8 POSS particles disperse well, are effective nucleating agents and increase overall crystallinity. In contrast Q_8 POSS particles become aggregated at high wt% loadings and hinder crystallization rates and reduce crystallinity.

Both Q_8 and T_8 POSS cage systems could potentially serve as nanoparticulate fillers in polyolefins, but with differing influences on polymer crystallization and morphology. Certainly, this may have industrially important implications in the processing of polyolefins. It is well known that PE has very fast crystallization kinetics,^{57–59} thus being able to hinder or nucleate crystallization rates at processing temperatures and hence alter the crystallinity and resulting morphology can allow tailoring of the material to application. However, the mechanical properties of the host polymer may well be significantly influenced by the changes in crystallinity and morphology which requires attention if POSS is to be employed as a nanoparticulate filler system. Further to this, experimental investigations into the mechanical properties of the POSS blends presented here are currently being undertaken and will be published by the authors in a forthcoming paper.

Acknowledgements

X-ray beam time was provided under the experimental application SM-6719. We are grateful for the assistance of all the Diamond I22 beamline staff. Mr Ian Williamson is acknowledged for assistance with sample preparation and experimental measurements. Mr Gordon Imlach is acknowledged for SEM sample preparation and instrumental analysis.

Notes and references

- 1 D. W. J. Scott, *J. Am. Chem. Soc.*, 1946, **68**, 356.
- 2 R. H. Baney, I. Itoh, A. Sakakibara and T. Suzuki, *Chem. Rev.*, 1995, **95**, 1409.
- 3 J. J. Schwab and J. D. Lichtenhan, *Appl. Organomet. Chem.*, 1998, **12**, 707.
- 4 J. Wu and P. T. Mather, *Polym. Rev.*, 2009, **49**, 25.
- 5 F. K. Wang, X. Lu and C. He, *J. Mater. Chem.*, 2011, **21**, 2775.
- 6 S. H. Phillips, T. S. Haddad and S. J. Tomczak, *Curr. Opin. Solid State Mater. Sci.*, 2004, **8**, 21.
- 7 S. W. Kuo and G. C. Chang, *Prog. Polym. Sci.*, 2011, **36**, 1649.
- 8 D. B. Cordes, P. D. Lickiss and F. Rataboul, *Chem. Rev.*, 2010, **110**, 2081.
- 9 G. Li, L. Wang, H. Ni and C. U. Pittman, *J. Inorg. Organomet. Polym.*, 2001, **11**, 123.
- 10 R. Y. Kannan, H. J. Salacinski, P. E. Butler and A. M. Seifalian, *Acc. Chem. Res.*, 2005, **38**, 879.
- 11 A. R. Bassindale and T. E. Gentle, *J. Mater. Chem.*, 1993, **12**, 1319.
- 12 R. M. Laine, *J. Mater. Chem.*, 2005, **15**, 3725.
- 13 N. Auner, B. Ziemer, B. Herrschaft, W. Ziche, P. John and J. Weis, *Eur. J. Inorg. Chem.*, 1999, **1999**, 1087.
- 14 E. Markovic, J. Matison, M. Hussain and G. P. Simon, *Macromolecules*, 2007, **40**, 4530.
- 15 F. X. Perrin, T. B. V. Nguyen and A. Margaille, *Eur. Polym. J.*, 2011, **47**, 1370.
- 16 E. L. Heeley, D. J. Hughes, Y. El Aziz, I. Williamson, P. G. Taylor and A. R. Bassindale, *Phys. Chem. Chem. Phys.*, 2013, **15**, 5518.
- 17 Y. C. Sheen, C. H. Lu, C. F. Huang, S. W. Kuo and F. C. Chang, *Polymer*, 2008, **49**, 4017.
- 18 B. X. Fu, L. Yang, R. H. Somani, S. S. Zong, B. S. Hsiao, S. Philips, R. Balanski and P. Ruth, *J. Polym. Sci., Part B: Polym. Phys.*, 2001, **39**, 2727.
- 19 A. Fina, D. Tabunani, A. Frache and G. Camino, *Polymer*, 2005, **46**, 7855.
- 20 A. J. Waddon, L. Zheng, R. J. Farris and E. B. Coughlin, *Nano Lett.*, 2002, **2**, 1149.
- 21 M. Joshi and B. S. Butona, *J. Appl. Polym. Sci.*, 2007, **105**, 978.
- 22 E. L. Heeley, D. J. Hughes, Y. El Aziz, P. G. Taylor and A. R. Bassindale, *Eur. Polym. J.*, 2014, **51**, 45.
- 23 J. Zeng, S. Kumar, S. Iyer, D. A. Schiraldi and R. I. Gonzalez, *High Perform. Polym.*, 2005, **17**, 403.
- 24 H. W. Milliman, H. Ishida and D. A. Schiraldi, *Macromolecules*, 2012, **45**, 4650.
- 25 E. T. Kopesky, T. S. Haddad, G. H. McKinley and R. E. Cohen, *Polymer*, 2005, **46**, 4743.
- 26 J. Wu, T. S. Haddad and P. T. Mather, *Macromolecules*, 2009, **42**, 1142.
- 27 E. S. Cozza, Q. Ma, O. Monticelli and P. Cebe, *Eur. Polym. J.*, 2013, **49**, 33.
- 28 R. Misra, B. X. Fu, A. Plagge and S. E. Morgan, *J. Polym. Sci., Part B: Polym. Phys.*, 2009, **47**, 1088.
- 29 R. Jeziórska, B. Świerz-Motysia, A. Szadkowska, B. Marciniak, H. Maciejewski, M. Dutkiewicz and I. Leszczyńska, *Polimery*, 2011, **56**, 809.
- 30 L. Matějka, A. Strachota, J. Pleštil, P. Whelan, M. Steinhart and M. Šlouf, *Macromolecules*, 2004, **37**, 9449.
- 31 K. N. Raftopoulos, M. Jancia, D. Aravopoulou, E. Hebda, K. Pielichowski and P. Pissis, *Macromolecules*, 2013, **46**, 7378.
- 32 J. H. Chen and Y. D. Chiou, *J. Polym. Sci., Part B: Polym. Phys.*, 2006, **44**, 2122.
- 33 M. Pracella, D. Chionna, A. Fina, D. Tabuani, A. Frache and G. Camino, *Macromol. Symp.*, 2006, **234**, 59.



- 34 A. Fina, D. Tabuani and G. Camino, *Eur. Polym. J.*, 2010, **46**, 14.
- 35 F. Baldi, F. Bignotti, A. Fina, D. Tabuani and T. Riccò, *J. Appl. Polym. Sci.*, 2007, **105**, 935.
- 36 A. N. Frone, F. X. Perrin, C. Radovici and D. M. Panaitescu, *Composites, Part B*, 2013, **50**, 98.
- 37 F. X. Perrin, D. M. Panaitescu, F. N. Frone, C. Radovici and C. Nicolae, *Polymer*, 2013, **54**, 2347.
- 38 E. L. Heeley, D. J. Hughes, Y. El Aziz, P. G. Taylor and A. R. Bassindale, *Macromolecules*, 2013, **46**, 4944.
- 39 L. Wang, Y. Ishida, R. Maeda, M. Tokita, S. Horiuchi and T. Hayakawa, *Langmuir*, 2014, **30**, 9797.
- 40 L. Wang, Y. Ishida, R. Maeda, M. Tokita and T. Hayakawa, *RSC Adv.*, 2014, **4**, 34981.
- 41 E. L. Heeley, A. C. Morgovan, W. Bras, I. P. Dolbnya, A. J. Gleeson and A. J. Ryan, *PhysChemComm*, 2002, **5**, 158.
- 42 M. Sentmanat, B. N. Wang and G. H. McKinley, *J. Rheol.*, 2005, **49**, 585.
- 43 E. L. Heeley, T. Gough, D. J. Hughes, W. Bras, J. Rieger and A. J. Ryan, *Polymer*, 2013, **54**, 6580.
- 44 X. Huang, L. Xie, P. Jiang, G. Wang and Y. Yin, *Eur. Polym. J.*, 2009, **45**, 2172.
- 45 J. Brandrup, E. H. Immergut and E. A. Grulke, *Polymer Handbook*, Wiley-Interscience, New York, 4th edn, 2003.
- 46 <http://www.diamond.ac.uk/Beamlines/Soft-Condensed-Matter/small-angle/I22.html>.
- 47 A. Berry, W. I. Helsby, B. T. Parker, C. J. Hall, P. A. Buksh, A. Hill, N. Clague, M. Hillon, G. Corbett, P. Clifford, A. Tidbury, R. A. Lewis, R. J. Cernik, P. Barnes and G. E. Derbyshire, *Nucl. Instrum. Methods Phys. Res., Sect. A*, 2003, **513**, 260.
- 48 J. E. Bateman, G. E. Derbyshire, G. Diakun, D. M. Duxbury, J. P. A. Fairclough, I. Harvey, W. I. Helsby, J. D. Lipp, A. S. Marsh, J. Salisbury, G. Sankar, E. J. Spill, R. Stephenson and N. J. Terrill, *Nucl. Instrum. Methods Phys. Res., Sect. A*, 2007, **530**, 1526.
- 49 W. Bras, I. P. Dolbnya, D. Detollenaere, R. van Tol, M. Malfois, G. N. Greaves, A. J. Ryan and E. Heeley, *J. Appl. Crystallogr.*, 2003, **36**, 791.
- 50 E. L. Heeley, C. M. Fernyhough, R. S. Graham, P. D. Olmsted, N. J. Inkson, J. Embery, D. J. Groves, T. C. B. McLeish, A. C. Morgovan, F. Meneau, W. Bras and A. J. Ryan, *Macromolecules*, 2006, **39**, 5058.
- 51 M. Avrami, *J. Chem. Phys.*, 1939, **7**, 1103.
- 52 M. Avrami, *J. Chem. Phys.*, 1940, **8**, 212.
- 53 G. F. Shan, W. Yang, X. G. Tang, M. B. Yang, B. H. Xie, Q. Fu and Y. W. Mai, *Polym. Test.*, 2010, **29**, 273.
- 54 Y. El Aziz, A. R. Bassindale, P. G. Taylor, R. A. Stephenson, M. B. Hursthouse, R. W. Harrington and W. Clegg, *Macromolecules*, 2013, **46**, 988.
- 55 M. Joshi, B. S. Butola, G. Simon and N. Kukaleva, *Macromolecules*, 2006, **39**, 1839.
- 56 M. Joshi and B. S. Butola, *Polymer*, 2004, **45**, 4953.
- 57 A. Sharples, *Introduction to Polymer Crystallization*, Edward Arnold Ltd., London, 1966.
- 58 U. W. Gedde, *Polymer Physics*, Springer, 1995.
- 59 J. M. Schultz, *Polymer Crystallization. The Development of Crystalline Order in Thermoplastic Polymers*, Oxford, New York, 2001.
- 60 L. Zheng, A. J. Waddon, R. J. Farris and E. B. Coughlin, *Macromolecules*, 2002, **35**, 2375.
- 61 D. Zhang, Y. Shi, Y. Liu and G. Huang, *RSC Adv.*, 2014, **4**, 41364.
- 62 D. Zhang, Y. Liu, Y. Shi and G. Huang, *RSC Adv.*, 2014, **4**, 6275.

